Cumhuriyet Sci. J., 46(4) (2025) 949-956
DOI: https://doi.org/10.17776/csj.1739508

Cumhuriyet Science Journal

| csj.cumhuriyet.edu.tr | Founded: 2002 ISSN: 2587-2680 e-ISSN: 2587-246X Publisher: Sivas Cumhuriyet University

Gamma Attenuation Properties of $SrTiO_3$ Doped with Rb and Y

Sümeyye Gümüş Uzun[1,a*], Hakan Eroğlu[1,b], Bayram Bilmez[2,c], Mustafa Çağatay Tufan[1,d], Mevlüt Gürbüz[3,e], Bilgehan Cem Turan[3,f]

[1]*Ondokuz Mayis University, Graduate School, Department of Radiological Sciences, 55139 Atakum, Samsun, Türkiye*

[2]*Ondokuz Mayis University, Faculty of Sciences, Department of Physics, 55139 Atakum, Samsun, Türkiye*

[3]*Ondokuz Mayis University, Faculty of Engineering, Department of Mechanical Engineering, 55139 Atakum, Samsun, Türkiye*

**Corresponding author*

Research Article

History
Received: 11/07/2025
Accepted: 14/10/2025

ABSTRACT

In this study, an experimental and theoretical study was carried out to investigate the radiation shielding properties of Strontium Titanate ($SrTiO_3$) perovskite ceramic with 1% Rb and Y added. For this purpose, nanocrystal samples of $SrTiO_3$: Rb and Y were synthesized by solid state reaction method. The gamma attenuation properties of Rb and Y doped $SrTiO_3$ were investigated by using narrow beam geometry gamma spectrometry system. In this study, linear and mass attenuation coefficients were determined for 0.1218 MeV, 0.2447, 0.3443, 0.7789, 0.964 and 1.408 MeV energy peaks of Eu-152 and from these values, atomic and electronic cross sections, half value thickness (HVL), tenth value thickness (TVL) and mean free path (MFP) values were also calculated. The results were compared with WinXCom values. It was found that Rb and Y doping increased the attenuation coefficients in the low energy region, but its effects were limited at higher photon energies. The same trend was observed for other calculated parameters such as HVL, TVL and MFP. It was found that $SrTiO_3$ perovskite samples with 1% Rb and Y doping had high attenuation properties and had good potential for shielding and other dosimetric uses. In this study, effective atomic number (Z_{eff}) and effective electron density (N_{eff}), which are important parameters in gamma absorption, were also calculated and compared with experimental results.

Keywords: Gamma attenuation coefficient, Scintillation detector, NaI(Tl), Strontium Titanate, Rare earth elements

[a] *sumeyye-gumus@hotmail.com* *https://orcid.org/0000-0003-1763-2373*
[b] *hakaneroglu55@gmail.com* *https://orcid.org/0009-0004-4072-1846*
[c] *bayram.bilmez@omu.edu.tr* *https://orcid.org/0000-0002-5687-2145*
[d] *mctufan@omu.edu.tr* *https://orcid.org/0000-0003-3110-5115*
[e] *mgurbuz@omu.edu.tr* *https://orcid.org/0000-0003-2365-5918*
[f] *bilgehancemturan@gmail.com* *https://orcid.org/0000-0001-8176-2995*

Introduction

With the widespread use of gamma rays in medical diagnoses, nuclear medicine, nuclear engineering and space technology, industry, and agriculture, the interaction of radiation with matter has become an important issue. Today, the increasing use of radiation has negative effects on human health. Long-term or high-dose exposure can lead to acute radiation syndrome, immune system suppression, and fatal consequences. Shielding is a protective application that is used to reduce or completely prevent the harmful effects of gamma (γ) rays on human health and the environment. Gamma rays are a type of high-energy electromagnetic radiation and have the ability to penetrate deeply. This makes them both dangerous and a type of radiation that requires shielding. Researchers have developed and produced many armor materials. Therefore, it is important to determine the attenuation properties of the material against high energy electromagnetic radiation. These properties depend on the composition of the material and the energy of the electromagnetic radiation; linear and mass attenuation coefficients (μ, μm), atomic (σt,a) and electronic (σt,e) interaction cross sections, effective atomic number (Zeff) and effective electron density (Neff). In addition, half value thickness (HVL), tenth value thickness (TVL) and mean free path (MFP) are important parameters that must be known to design and select a shielding material. The interaction between gamma ray and matter depends on the incident photon energy and target material's composition. Gamma ray interacts with matter by mechanisms such as photoelectric effect, Compton scattering and pair production. These interaction mechanisms cause the attenuation of the incident beam of gamma ray.

$SrTiO_3$ is a perovskite compound with moderate gamma-ray absorption, used in a wide range of applications due to its high dielectric constant, wide band gap, structural stability and versatile doping possibilities. Due to its high dielectric constant, it is widely used in capacitors, particularly in DRAMs and integrated circuits. Additionally, it serves as a resonator material in microwave devices and radio frequency applications [1]. Doping $SrTiO_3$, for instance with niobium (Nb), enhances its thermoelectric properties by inducing semiconducting behavior. Moreover, under appropriate doping, $SrTiO_3$ can exhibit superconductivity at very low temperatures Its wide band gap (~3.2 eV) makes it a promising candidate for photocatalytic water splitting and solar-driven hydrogen production, contributing to environmentally

friendly energy solutions[2]. $SrTiO_3$ also demonstrates a moderate gamma-ray attenuation capability. It is utilized as a filler material in polymer matrices to develop lightweight radiation shielding materials. As a lead-free and non-toxic compound, it offers a sustainable alternative to traditional shielding materials. $SrTiO_3$ is weak compared to high-Z materials, but its stability and processability make it useful in developing secondary protective layers or lead-free alternatives [3-5]. It is especially valuable in applications where environmentally friendly, non-toxic and durable materials are sought.

$SrTiO_3$ is a ceramic material with a perovskite crystal structure, which exhibits high thermal and chemical stability under radiation exposure. This structural resilience allows the material to maintain its integrity and functionality in high-radiation environments, making it particularly advantageous for use in nuclear reactors, space applications, and medical radiation shielding. The $SrTiO_3$ compound is a promising candidate for gamma radiation shielding due to the presence of strontium (Z=38) and titanium (Z= 22), which contribute significantly to photon–matter interactions, particularly via the photoelectric effect and Compton scattering [6]. The relatively high atomic numbers of these constituent elements, along with the compound's dense ceramic structure, enhance its gamma-ray attenuation capability. Furthermore, $SrTiO_3$ offers a non-toxic and thermally stable alternative to conventional shielding materials such as lead. Compared to conventional gamma shielding materials such as lead (Pb), $SrTiO_3$ is non-toxic and environmentally friendly. It offers a lighter, more chemically stable, and more easily processable alternative to lead-based materials. Additionally, $SrTiO_3$ exhibits dielectric and piezoelectric properties, enabling multifunctional applications beyond radiation shielding. The gamma attenuation capability of $SrTiO_3$ is particularly significant for low- to medium-energy gamma photons. While high-Z materials like lead are more effective at higher photon energies, $SrTiO_3$ provides a safer and more sustainable solution for many radiation shielding scenarios where reduced toxicity and structural flexibility are desired.

Rubidium (Rb) is a highly reactive alkali metal with distinct physical and chemical properties, including a low melting point and photoelectric sensitivity. Due to its reactivity and rarity, its applications are limited to specialized fields.One of its primary uses is in rubidium atomic clocks, which provide high-precision timekeeping for GPS and satellite systems [7]. In quantum physics, rubidium atoms are cooled to form Bose–Einstein condensates, allowing the study of quantum phenomena [8]. In medical imaging, the isotope Rb-82 is used in PET scans to evaluate cardiac function. Additional uses include photoelectric sensors, specialty glass, and flame photometry, where rubidium produces a characteristic reddish-violet flame [9]. Although industrial use is rare, rubidium remains important in research, precision instruments, and medical diagnostics.

Yttrium (Y) is a silvery-white, relatively soft rare-earth metal (atomic number 39, stable isotope Y-89) with a high melting point (~1,522 °C). Its diverse properties enable a wide range of applications in electronics, materials science, medicine, and energy [10]. Yttrium is chemically and physically similar to the lanthanides and is usually found with them in nature, so it is classified as a rare earth element. However, it is not technically a lanthanide because its atomic number and period differ from those of the lanthanides [11]. The radioactive isotope Y-90 is used in cancer treatments (radioembolization, brachytherapy) and some PET/SPECT imaging techniques. The stable isotope Y-89 is being studied for advanced imaging methods like NMR and MRI [12].

The aim of this study is to determine the gamma ray attenuation properties of the SrTiO3 doped with Rb+ (1% mol) and Y+3 (1% mol) and to pave the way for new application areas especially in radiation shielding applications. To minimize the effect of dopant, doped ratio was kept at 1% mol. For this purpose linear and mass attenuation parameters were determined by using gamma spectrometry system, then other parameters, such as atomic and electronic cross sections, effective atomic number and electron density, were calculated. Obtained results were compared well known database NIST XCOM.

Materials and Methods

Sample Preparation

In this study, Rb+ and Y+3 doped SrTiO3 samples were prepared using the solid-state synthesis method. Compared to other processes, the solid state synthesis method has advantages in terms of low production costs and simplicity of production process. The doping rate is 1% for both elements. Commercial powder forms of these elements were mixed using stoichiometric ratios to prepare the samples. These powders were placed in the grinding chamber with 50 mL of ethyl alcohol and zircon balls (50 balls used, and each was 1 g) to achieve a homogeneous dissolution, then left in the mill, rotated at 150 rpm for 24 hours. The dissolved materials from the grinding chamber were dried in the oven at 70 °C for 20 hours. The dried materials were crushed in an agate mortar and then sieved. The materials were placed in the oven for the first heat treatment at 1200°C for 2 hours (the heating rate was 5 °C/m), and at the end of the process, they were crushed again in an agate mortar and sieved. Powder samples were pressed under high pressure to obtain 10x10x2 mm pellets.

Gamma attenuation parameters

When a gamma-ray beam passes through an absorber, the intensity of the beam will attenuate according to exponential law [13]:

$$I = I_0\, exp(-\mu x) \tag{1}$$

Radiation attenuation refers to the decrease in radiation intensity as it passes through a material. Here I and I0 are the attenuated and incident gamma ray intensities, respectively. Accordingly, the change in radiation intensity is directly proportional to the initial intensity and the armor thickness, but has the opposite sign since it decreases [14, 15]. Here, x is the thickness of the sample in cm, μ is the mass attenuation coefficient of the medium and depends on the energy of the radiation and the density of the medium (ρ).

There are also three fundamental quantities that are important for radiation attenuation: the half-value thickness (HVL), which attenuates the initial intensity of the incident photons by half; tenth value thickness (TVL), which attenuates the initial intensity to one tenth, and mean free path (MFP), which is the distance a photon travels betwwen two interaction:

$$HVL = \frac{0.693}{\mu} \quad (2)$$

$$TVL = \frac{2.3026}{\mu} \quad (3)$$

$$MFP = \frac{1}{\mu} \quad (4)$$

For a multi-element medium, the atomic and electronic cross sections can be found using the mass attenuation coefficients as follows [16]:

$$\sigma_{t,a} = \frac{\mu_m}{N_A \sum_i \frac{\omega_i}{A_i}} \quad (5)$$

and

$$\sigma_{t,e} = \frac{1}{N_A} \sum \frac{f_i A_i}{Z_i} (\mu_m)_i \quad (6)$$

Here NA is the Avogadro constant, fi, Ai and Zi are the number of ith elements relative to the total number of atoms of all elements in the mixture, their atomic weights (in grams) and the atomic number of the ith element.

The effective atomic number (Zeff) and effective electron number (Neff) of a multi-element medium is determined from the total atomic cross section and electronic cross section as follows [17-19]:

$$Z_{eff} = \frac{\sigma_{t,a}}{\sigma_{t,e}} \quad (7)$$

$$N_{eff} = \frac{\mu_m}{\sigma_{t,e}} \quad (8)$$

Experimental Setup

The detection of γ rays was carried out using a gamma spectrometer system consisting of a 10 cm diameter NaI(Tl) detector connected to a Multi-Channel Analyzer (MCA). Gamma spectrometry allows direct, non-destructive and rapid analysis of the radionuclide composition of the sample. The detector efficiency is 2% at 0.5 MeV and 1.3% at 2 MeV. The experimental setup is shown in Figure 1. Since the narrow beam geometry is used, the distance between the sample and the detector is kept at a distance sufficient for only the gamma rays scattered below 1 degree to reach the detector. Experiments were carried out for Eu-152 gamma rays at 0.1218, 0.2447, 0.3443, 0.7789, 0.964 and 1.408 MeV. Since the samples were thin and collimation was intense, the counting time was kept at 6 hours in order to increase the counting statistics and 1% uncertainty was obtained. The mass attenuation coefficients (μ/ρ) with the known density (ρ) of a material were obtained by measuring the linear attenuation coefficients. Theoretical μ/ρ values for the available samples were obtained with the WinXCom program [20].

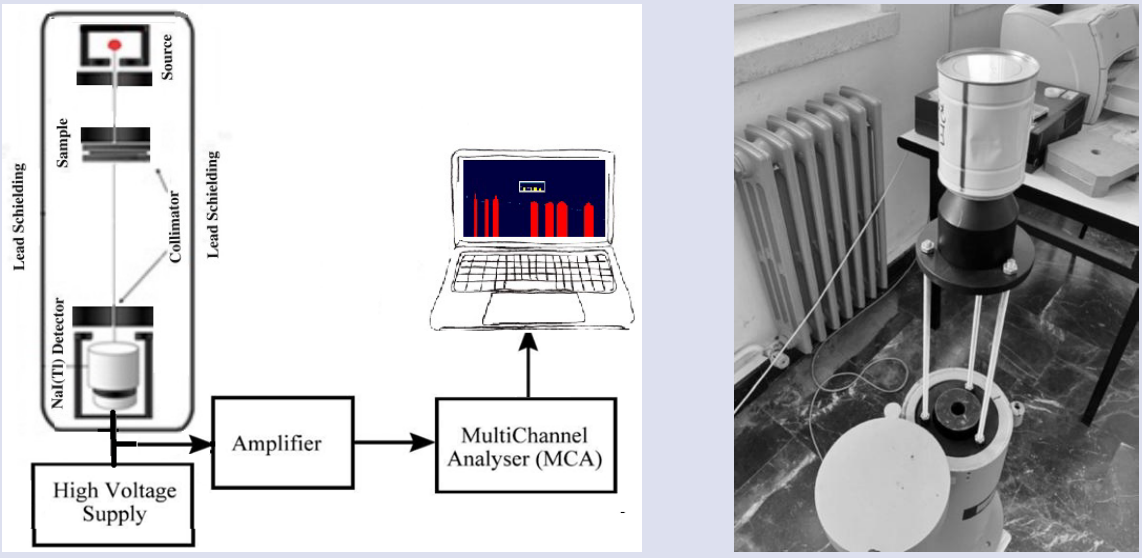

(a) (b)

Figure 1. (a) The experimental setup with NaI(Tl) scintillation detector, (b) Eu-152 radioactive source and narrow beam collimator in site fotograph.

Results and Dıscussıon

As a first step, mass densities of the prepared samples were determined using Archimedes' principle. For this, we used purified water and measured the sample's weight and buoyant force in the water. The obtained densities are given in Table 1. The numbers at the end of the sample name correspond to the percentage contribution of the Rb and Y.

Table 1. Densities of the samples

Sample	Density (g/cm^3)
$SrTiO_3$:Rb1	1.79±0.017
$SrTiO_3$:Y1	3.76±0.085

Attenuation parameters were determined by applying Eq.1. For this purpose experimental was set as shown in Fig.1, and incident and attenuated intensities were determined. Obtained results are shown together with the NIST XCOM values [20] in Table 2. Table 1 and 2 also show the systematic erros in the measured data caused by the instruments.

Figures 2a and b present the mass attenuation coefficients as a function of photon energy for Rb- and Y-doped strontium titanate, respectively. The total mass attenuation coefficients were derived from theoretical models, incorporating major photon interaction processes, including coherent (Rayleigh) scattering, incoherent (Compton) scattering, photoelectric absorption, and pair production in both nuclear and electric fields. The experimental data points are also included for comparison.

At low photon energies (below 0.1 MeV), the dominant interaction mechanism is photoelectric absorption. As expected, the mass attenuation coefficient sharply decreases with increasing photon energy due to the inverse energy dependence of the photoelectric effect. This can be seen both theoretical (XCOM) and experimental results in Fig.2.

In the intermediate energy range (0.1–3 MeV), Compton scattering becomes the dominant interaction process for both materials. The curves for incoherent scattering exhibit a broad peak in this region, indicating the prevalence of this mechanism. The similarity in the Compton scattering contributions between the two samples suggests that this process is less sensitive to the specific dopant compared to the photoelectric effect.

At higher energies pair production in the nuclear and electric fields becomes significant. Both SrTiO3: Rb1 and SrTiO3: Y1 exhibit similar trends in this region, with a gradual increase in the total mass attenuation coefficient due to the onset of pair production.

Notably, the total attenuation coefficients including coherent scattering closely follow the experimental measurements across the entire energy range for both doped materials. The minor discrepancies observed at certain energies may be attributed to limitations in the theoretical cross-section models or slight variations in material composition.

Experimental results were compared with theoretical mass attenuation coefficients obtained from the NIST XCOM database. The deviation between experimental and theoretical values is generally within ± 7% indicating strong agreement. The slightly larger discrepancy observed at 0.3443 MeV for SrTiO3:Rb1 may stem from experimental uncertainties or material inhomogeneities. At all measured energies, the experimental values for both materials track the trends predicted by XCOM data, validating the reliability of the experimental methodology and sample preparation.

Table 2. Experimental linear and mass attenuation coefficients of the samples and theoretical mass attenuation coefficients from WinXCom database.

$SrTiO_3$:Rb1			
Energy (MeV)	**μ (1/cm)**	**μ_m (cm^2/g)**	**NIST XCOM μ_m (cm^2/g)**
0.1218	0.6176±0.0374	0.3454±0.0242	0.34350
0.2447	0.2433±0.0196	0.1361±0.0123	0.13480
0.3443	0.1491±0.0094	0.0834±0.0061	0.10470
0.7789	0.1121±0.0094	0.0627±0.0058	0.06735
0.964	0.1096±0.0091	0.0613±0.0057	0.06043
1.408	0.0887±0.0060	0.0496±0.0038	0.04973
$SrTiO_3$:Y1			
Energy (MeV)	**μ (1/cm)**	**μ_m (cm^2/g)**	**NIST XCOM μ_m (cm^2/g)**
0.1218	1.3722±0.1140	0.3650±0.0385	0.34430
0.2447	0.5268±0.0538	0.1401±0.0175	0.13490
0.3443	0.3749±0.0324	0.0997±0.0109	0.10470
0.7789	0.2606±0.0283	0.0693±0.0091	0.06737
0.964	0.2360±0.0245	0.0628±0.0079	0.06044
1.408	0.1789±0.0162	0.0476±0.0054	0.04973

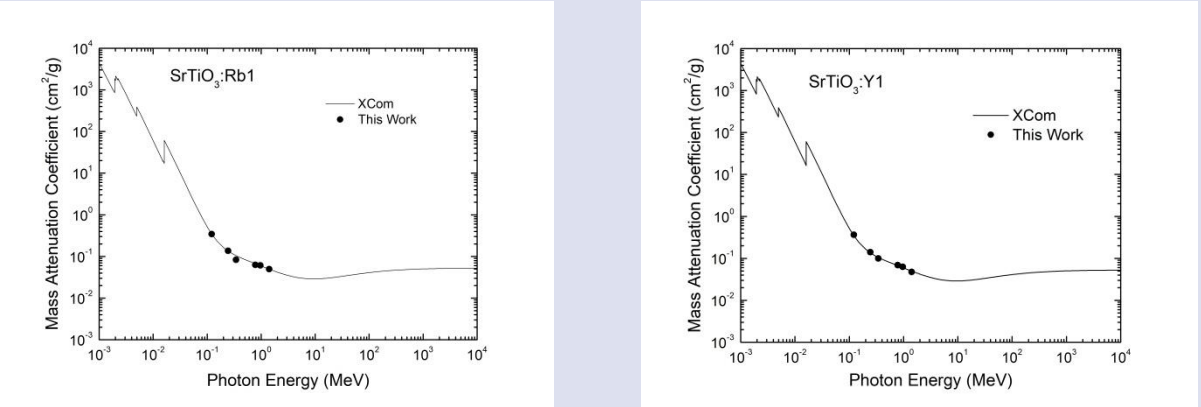

(a) (b)

Figure 2. Mass attenuation coefficients in the energy range of 0.001 MeV to 10 MeV for (a) $SrTiO_3$:Rb1 and (b) $SrTiO_3$:Y1

To further assess the photon interaction behavior and shielding potential of $SrTiO_3$-based materials, several key parameters were calculated: atomic and electronic cross sections, effective atomic number, effective electron density, half-value layer (HVL), tenth-value layer (TVL), and mean free path (MFP). These values are summarized in Table 3 and shown in Figs.3-6. for $SrTiO_3$:Rb1 and $SrTiO_3$:Y1, respectively.

The effective atomic number is an important indicator of the material's interaction probability with photons, particularly in the photoelectric region. At low photon energies (e.g., 0.1218 MeV), $SrTiO_3$:Y1 exhibits a slightly higher Zeff than $SrTiO_3$:Rb1 indicating stronger photon interaction due to the heavier Y dopant compared to Rb. Correspondingly, the effective electron density is higher for $SrTiO_3$:Y1 across most energy values, reflecting a higher electron population available for photon interactions. These variations are expected as they result from the differing electronic configurations and atomic weights of the dopants.

The macroscopic attenuation parameters, HVL, TVL, and MFP, provide a direct measure of the material's radiation-shielding capability. At 0.1218 MeV, $SrTiO_3$:Y1 has an HVL of 0.505 cm, significantly lower than 1.122 cm for $SrTiO_3$:Rb1, indicating better attenuation capability in the low-energy region. Similar trends are observed, with $SrTiO_3$:Y1 showing superior performance. Lower values for MFP in $SrTiO_3$:Y1 across all energies suggest more efficient attenuation, particularly at lower energies.

Table 3. Gamma interaction parameters for the samples

$SrTiO_3$:Rb1							
Energy (MeV)	**σ_a (cm^2/atom)**	**σ_e (cm^2/atom)**	**Z_{eff}**	**N_{eff}**	**HVL (cm)**	**TVL (cm)**	**MFP (cm)**
0.1218	2.11114E-23	8.42576E-25	25.05574255	4.09934E+23	1.122085492	3.728303109	1.619170984
0.2447	8.31863E-24	4.32106E-25	19.25136345	3.14969E+23	2.848335388	9.464036169	4.110152076
0.3443	5.09753E-24	2.88533E-25	17.66704290	2.89048E+23	4.647887324	15.44332663	6.706908115
0.7789	3.83232E-24	2.41372E-25	15.87722796	2.59765E+23	6.181980375	20.54058876	8.920606601
0.964	3.74675E-24	2.17402E-25	17.23416355	2.81966E+23	6.132743363	20.37699115	8.849557522
1.408	3.03163E-24	1.79314E-25	16.90679323	2.7661E+23	7.812852311	25.95941375	11.27395716
			$SrTiO_3$:Y1				
Energy (MeV)	**σ_a (cm^2/atom)**	**σ_e (cm^2/atom)**	**Z_{eff}**	**N_{eff}**	**HVL (cm)**	**TVL (cm)**	**MFP (cm)**
0.1218	2.23135E-23	8.43077E-25	26.46679041	4.32938E+23	0.505028422	1.678035272	0.728756741
0.2447	8.56473E-24	4.33221E-25	19.76989543	3.23392E+23	1.315489749	4.370918755	1.898253607
0.3443	6.09496E-24	3.57340E-25	17.05648358	2.79006E+23	1.848492931	6.141904508	2.667377967
0.7789	4.23652E-24	2.41270E-25	17.55926051	2.87231E+23	2.515426497	8.357894737	3.629764065
0.964	3.83915E-24	2.17338E-25	17.66445381	2.88951E+23	2.748909163	9.133677112	3.966679889
1.408	2.90993E-24	1.79208E-25	16.23769259	2.65613E+23	3.873672443	12.87087759	5.589714925

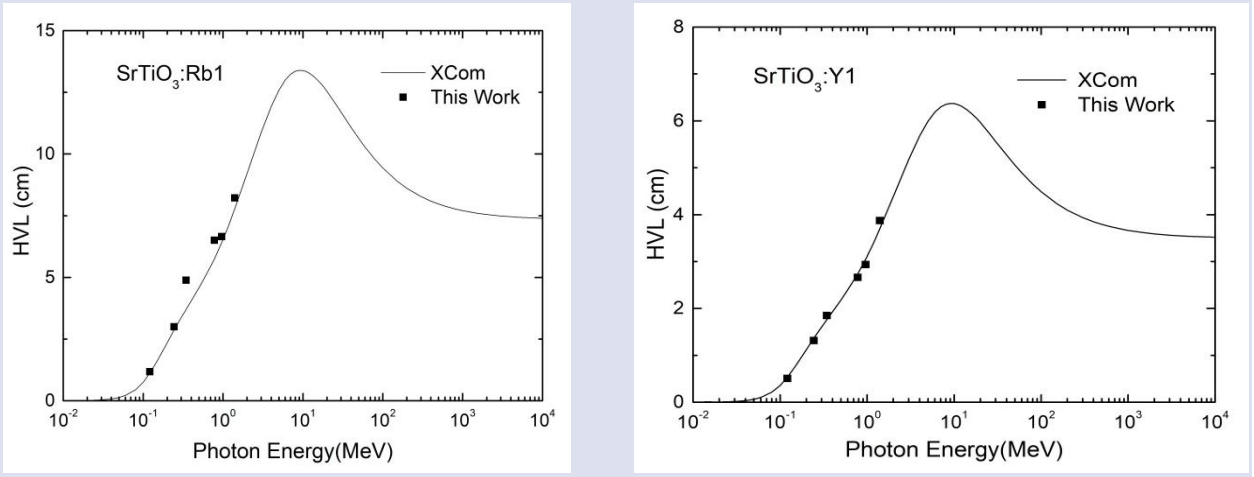

(a)

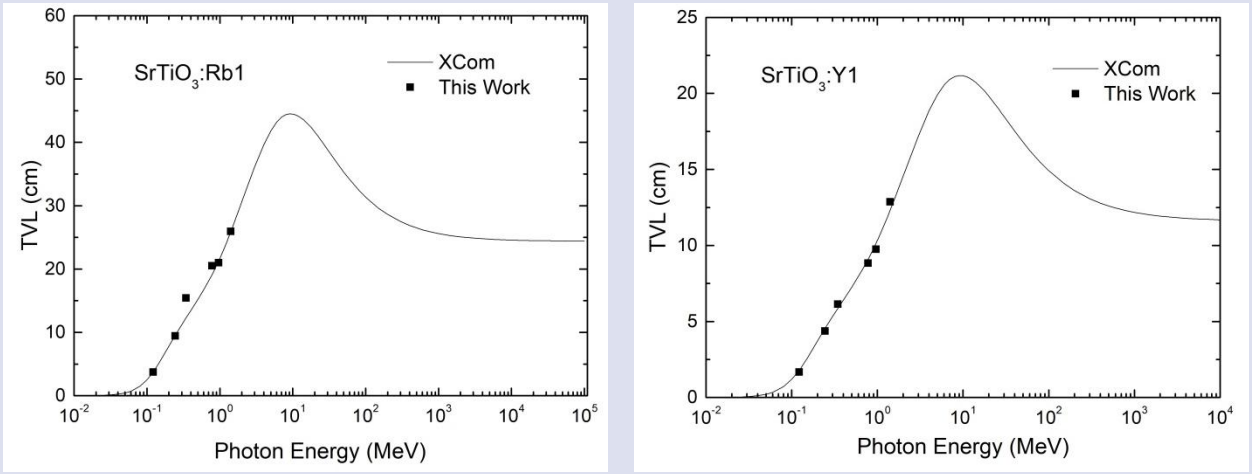

(b)

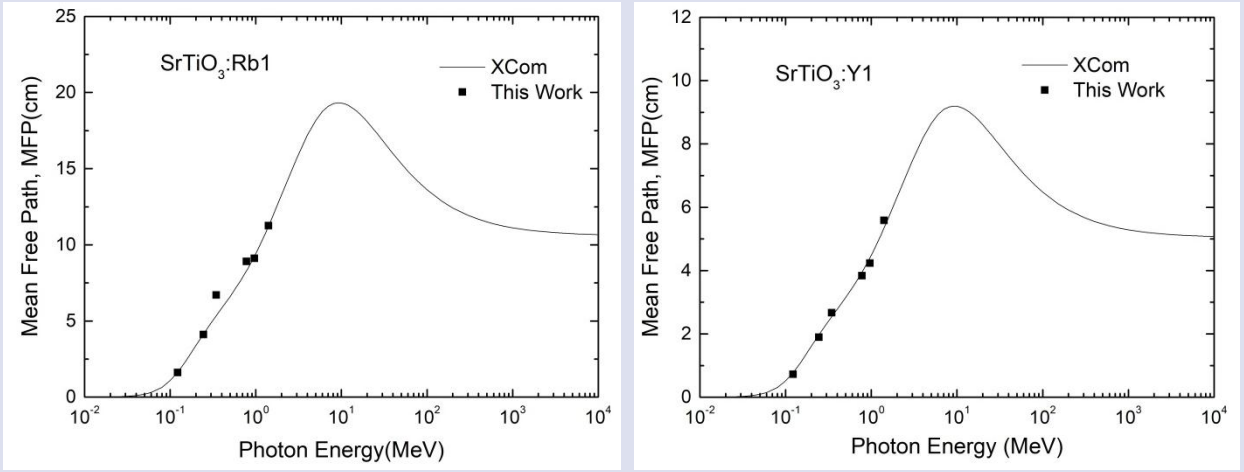

(c)

Figure 3. (a) Half value layer, (b) tenth value layer and (c) mean free path values in the energy range of 0.01 MeV to 10 MeV for $SrTiO_3$:Rb1 and $SrTiO_3$:Y1

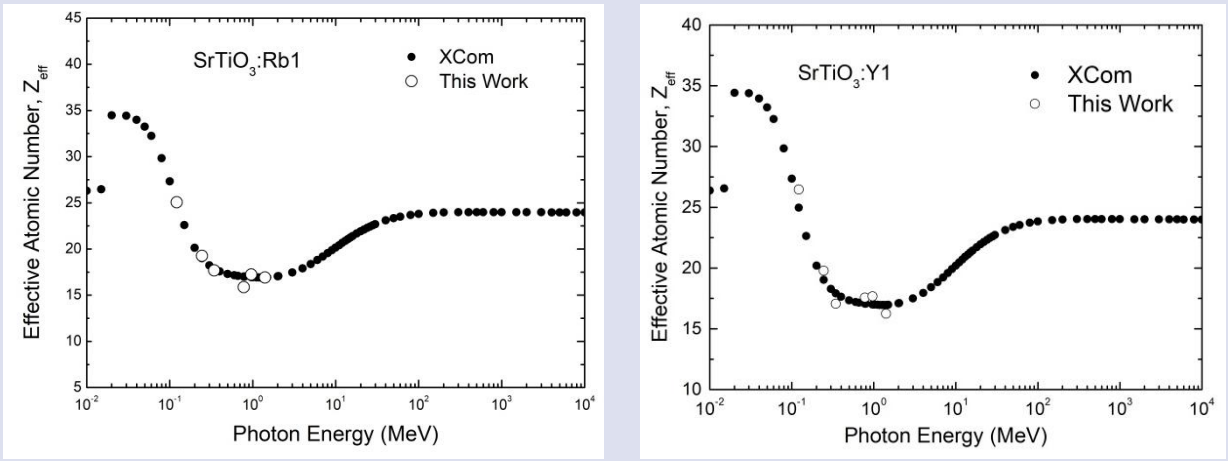

(a) (b)

Figure 4. Variation of effective atomic number with photon energy for (a) $SrTiO_3$:Rb1, (b) $SrTiO_3$:Y1 in the energy range of 0.01 MeV to 10 MeV.

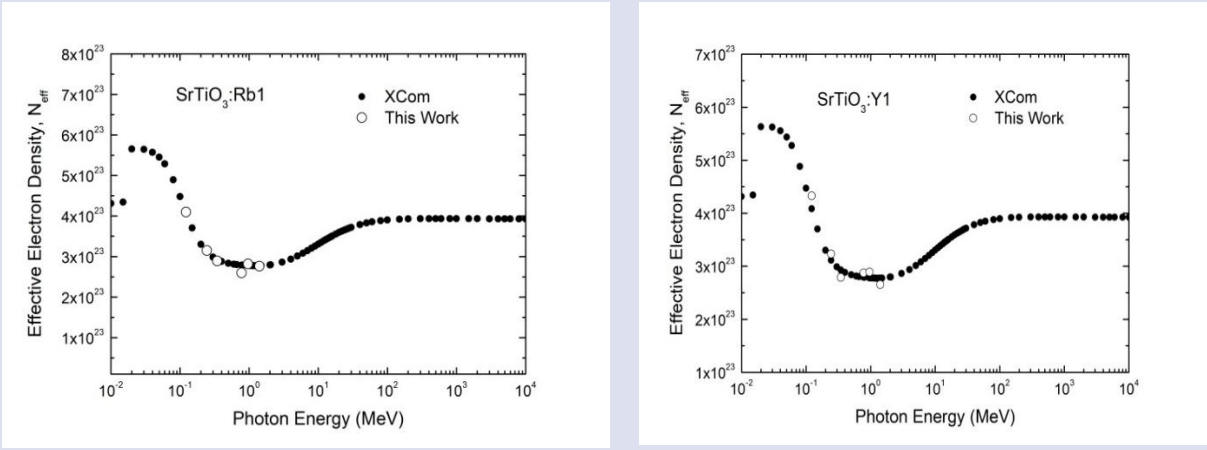

(a) (b)

Figure 5. Variation of effective electron number with gamma photon energy for (a) $SrTiO_3$:Rb1, (b) $SrTiO_3$:Y1 in the energy range of 0.01 MeV to 10 MeV.

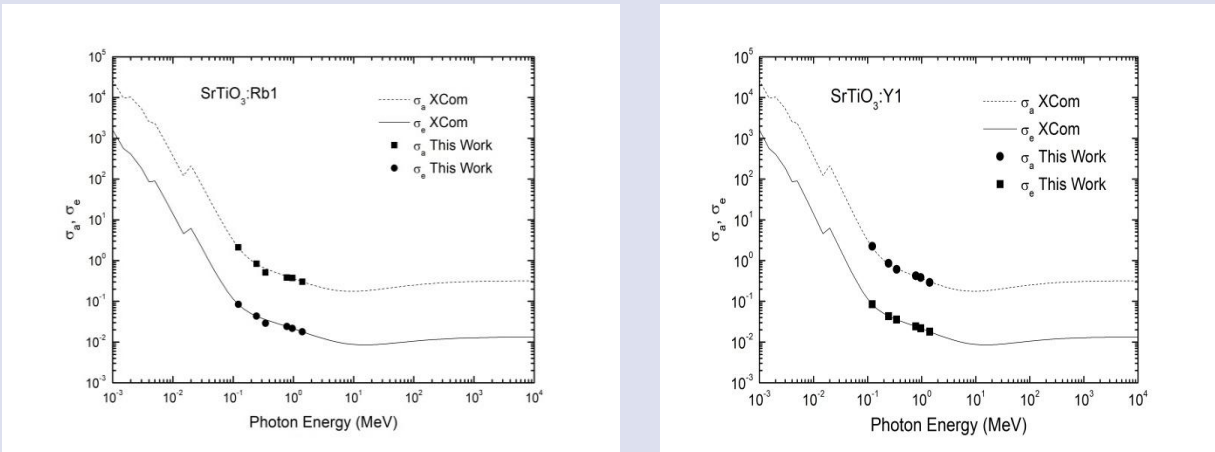

(a) (b)

Figure 6. Variation of atomic cross sections and electronic cross sections with gamma photon energy for (a) $SrTiO_3$:Rb1, (b) $SrTiO_3$:Y1 in the energy range of 0.001 MeV to 10 MeV.

When compared with water and tissue (Zeff around 3.5 in this energy range), it can be argued that the samples are not tissue equivalent. On the contrary, the samples have very strong gamma attenuation properties, opposing the low atomic number compounds such as water. The HVL of water and tissue is on the order of 4 cm in the 0.1 keV energy, whereas the samples investigated in this work have HVL values around 0.8 cm. Both a high effective number and a high mass density of the samples make this difference possible. These facts can be of advantage in certain shielding and radiation monitoring applications. As the low-energy gamma radiation is easily attenuated, very high efficiency can be expected with the SrTiO3 samples even in quite small volumes.

Conclusion

This study investigates gamma-ray interaction parameters of SrTiO3 doped with Rb and Y. For this purpose, samples were prepared using the solid-state synthesis method. 1% mol doping rate is used for both Rb and Y. The linear and mass attenuation coefficients of the samples in the energy range of 0.1218 to 1.406 were determined, and the results were compared with theoretical XCom values, and good agreement was observed. Even though the doping rates were modest, their effect is considerable in the low-energy region. It is found that Rb and Y doping increased the attenuation coefficients in the lower energy region and had little impact on the higher energy region. HVL, TVL, and MFP also illustrated a similar pattern. When dopants were added, their HVL and TVL values dropped, stemming from stronger gamma attenuation. It is well known that the attenuation of gamma beams is related to the sample's atomic number and electron density. The Zeff and Neff values also showed consistent results with theoretical calculations. By comparing the tissue equivalent substances, it has found that investigated samples have high Zeff. Thus, it can be concluded that the materials show a desirable interaction profile for low-energy photon radiation fields.

These results highlight the influence of high-Z dopants on photon interaction mechanisms, particularly in the low-energy domain, and suggest potential optimization strategies for radiation shielding or detector applications using perovskite-based compounds. Further studies on other dosimetric evaluations, such as charged particle interaction as well as luminescence properties, would be interesting. In future studies, it will be interesting to investigate how changing the doping percentage and type affects radiation shielding and luminescence properties. In this study, only the radiation shielding properties of the materials and their densities were determined using the Archimedes principle. It is observed that the densities differ from the expected values. It is important to also conduct structural and morphological studies of the materials to elucidate the reason for this.

Conflicts of interest

There are no conflicts of interest in the publication.

References

[1] Shim, J. H., Choi, H. J., Kim, Y., Torgersen, J., An, J., Lee, M. H., & Prinz, F. B. (2017). Process–property relationship in high-k ALD SrTiO3 and BaTiO3: a review. *Journal of Materials Chemistry C*, 5(32), 8000-8013.

[2] Popuri, S. R., Scott, A. J. M., Downie, R. A., Hall, M. A., Suard, E., Decourt, R., ... & Bos, J. W. (2014). Glass-like thermal conductivity in SrTiO3 thermoelectrics induced by A-site vacancies. *RSC Advances*, 4(64), 33720-33723.

[3] Guo, H., Dong, N., Yin, M., Zhang, W., Lou, L., & Xia, S. (2006). Green and red upconversion luminescence in Er3+-doped and Er3+/Yb3+-codoped SrTiO3 ultrafine powders. *Journal of Alloys and Compounds*, 415(1-2), 280-283.

[4] Deltreggia, L. A., Bernardi, M. I. B., & Mesquita, A. (2018). Influence of La substitution on local structural and photoluminescence properties of SrTiO3: Pr phosphor. *Scripta Materialia*, 157, 15-18.

[5] Melo, D. M. A., César, A., Martinelli, A. E., Silva, Z. R., Leite, E. R., Longo, E., & Pizanni, P. S. (2004). Room temperature photoluminescence of amorphous BaxSr1− xTiO3 doped with chromium. *Journal of Solid State Chemistry*, 177(3), 670-674.

[6] Sayyed, M. I., Hashim, S., Hannachi, E., Slimani, Y., & Elsafi, M. (2022). Effect of WO3 nanoparticles on the radiative attenuation properties of SrTiO3 perovskite ceramic. *Crystals*, 12(11), 1602. *(Cilt ve sayı bilgisi eklendi)*.

[7] Vanier, J., & Audoin, C. (1989). *The Quantum Physics of Atomic Frequency Standards*. CRC Press.

[8] Anderson, M. H., Ensher, J. R., Matthews, M. R., Wieman, C. E., & Cornell, E. A. (1995). Observation of Bose-Einstein condensation in a dilute atomic vapor. *Science*, 269(5221), 198-201.

[9] Lide, D. R. (2004). *CRC Handbook of Chemistry and Physics* (85. Baskı). CRC Press.

[10] Greenwood, N. N., & Earnshaw, A. (1997). *Chemistry of the Elements*. Butterworth-Heinemann.

[11] Kittel, C. (2004). *Introduction to Solid State Physics* (8. Baskı). Wiley.

[12] Tickner, B. J., Stasiuk, G. J., Duckett, S. B., & Angelovski, G. (2020). The use of yttrium in medical imaging and therapy: historical background and future perspectives. *Chemical Society Reviews*, 49(17), 6169-6185.

[13] Elmahroug, Y., Tellili, B., & Souga, C. (2015). Determination of total mass attenuation coefficients, effective atomic numbers and electron densities for different shielding materials. *Annals of Nuclear Energy*, 75, 268-274.

[14] Bashter, I. I. (1997). Calculation of radiation attenuation coefficients for shielding concretes. *Annals of Nuclear Energy*, 24(17), 1389-1401.

[15] Gülbiçim, H., Tufan, M. Ç., & Türkan, M. N. (2017). The investigation of vermiculite as an alternating shielding material for gamma rays. *Radiation Physics and Chemistry*, 130, 112-117.

[16] Akkurt, I., & El-Khayatt, A. M. (2013). Effective atomic number and electron density of marble concrete. *Journal of Radioanalytical and Nuclear Chemistry*, 295(1), 633-638.

[17] Prasad, S. G., Parthasaradhi, K., & Bloomer, W. D. (1998). Effective atomic numbers for photoabsorption in alloys in the energy region of absorption edges. *Radiation Physics and Chemistry*, 53(5), 449-453.

[18] Gümüş, H., Mhanna, S., & Gümüş Uzun, S. (2019). Investigation of Gamma-ray attenuation coefficients for some different tissues. *ALKÜ Fen Bilimleri Dergisi*, 1(2), 101-106. *(Cilt/Sayı eklendi)*.

[19] Gulbicim, H., Akan, H., & Tufan, M. C. (2025). Determination of X-ray Photon Absorption Properties of Some Human Tissues and Organs Using Monte Carlo method. *Indian Journal of Pure & Applied Physics (IJPAP)*, 63(2), 132-143. *(Cilt/Sayı eklendi)*.

[20] Berger, M. J., Hubbell, J. H., Seltzer, S. M., Chang, J., Coursey, J. S., Sukumar, R., ... & Olsen, K. (2010). *XCOM: Photon Cross Sections Database* (Versiyon 1.5). NIST.